

GBT X-band (9.6 GHz): All Sky Pointing

Dana S. Balser, Ronald J. Maddalena, Frank Ghigo, & Glen I. Langston

30 January 2002

Abstract

All sky pointing observations at X-band are discussed. A traditional pointing model including eight physical terms are used to fit the data. The all sky *rms* is 7".4.

1 Introduction

All sky pointing observations were made at X-band at a frequency of 9.6 GHz. These observations were performed with a new focus tracking model which included tilts of the sub-reflector (GBT Com. Memo 18) and a refined model for refraction (GBT Com. Memo 16). The observations were made continuously over a weekend and are discussed in §2. The data are divided by day and night and analyzed both separately and combined. The results are given in §3. The conclusions are in §4.

2 Observations and Analysis

Observations were made during 2001 December 28–30 (project = point_xband.04). All pointing sources were selected from the NVSS pointing calibrator list (Condon & Yin 2001, PASP, 113, 362). At 9.6 GHz the GBT half-power beam-width (HPBW) is 1'.25. The observing table "allsky_xband.obs" was created with the CLEO application *scheduler* using slew rates of 25°/0 per minute in azimuth with an acceleration time of 0.2 minute, and 18°/0 per minute in elevation with an acceleration time of 0.09 minute¹. Only sources brighter than 2 Jy at 9 GHz were selected. Here we assume that $F_\nu \propto \nu^{-0.7}$. A procedure time of 2 minutes was estimated which includes overhead time.

¹These reduced slew rates have now been increased to their nominal values of 40°/0 per minute in azimuth and 20°/0 per minute in elevation.

Both the Gregorian focus tracking model and the refraction model were refined and updated before the X-band all sky pointing run (see GBT Com. Memos 16 and 18). The three translational motions of the sub-reflector (X , Y , Z) were empirically determined² to be

$$X = 212.55 - 301.98 \cos(E) - 25.55 \sin(E) \text{ mm}, \quad (1)$$

$$Y = -148.39 + 183.74 \cos(E) + 9.96 \sin(E) \text{ mm}, \quad (2)$$

and

$$Z = 9.56 + 11.18 \cos(E) - 21.86 \sin(E) \text{ mm}. \quad (3)$$

The sub-reflector was then tilted in an attempt to further optimize the gain. It was determined that $X_t = -0^\circ 13 \pm 0.08$, $Y_t = 0^\circ 0$, and $Z_t = -0^\circ 058 \pm 0.03$ were optimal values. During these focus tracking observations it was noted that there exists a temperature dependence. This effect is larger along the axial direction (Y) than along the lateral X direction which coupled with pointing. Nonetheless, the predicted change in X is 5 mm per 10 Celsius which corresponds to a pointing error of 18", assuming a plate scale of 3"6 per millimeter.

The GO procedure *peak* was used to determine local pointing corrections (LPCs). The procedure *peak* performs two raster scans in RA ($W \rightarrow E$ and then $E \rightarrow W$). The procedure then pauses. An event is sent to an AIPS++ client which fills the data using *gbtmsfiller*, and then calculates the LPCs. If acceptable the LPCs are updated automatically and then the procedure performs two raster scans in Dec ($S \rightarrow N$ and then $N \rightarrow S$). Again the data are filled, analyzed, and the LPCs updated pending user verification. A telescope rate of 45' per minute was used with a length of 15' and an integration time of 0.15 s.

The data were analyzed using the AIPS++ DCR tool offline. The procedure *Point1* performs a first-order polynomial baseline fit using the first and last 10% of the scan, subtracts this model from the data, and then fits a Gaussian model to the resulting profile. The observed source position ($A_{\text{obs}}, E_{\text{obs}}$) is determined from the center position of the Gaussian model profile. The NVSS source J2000 equatorial coordinates are converted into horizon coordinates at the midpoint of the scan and are denoted as (A_*, E_*). The local pointing offset is just the difference between these two coordinates. Therefore,

$$\Delta A = A_{\text{obs}} - A_* \quad (4)$$

and

²The allowed motion in the focus tracking Z direction is still not sufficient to observe significant changes in the gain even at X-band. Therefore, the equation for Z is based on theodolite measurements of the feedarm.

$$\Delta E = E_{\text{obs}} - E_{*}. \quad (5)$$

The new LPCs are just the old values plus the local pointing offset determined in Equations (4) and (5).

The indicated telescope position is the difference between the know source position and the measured position. Therefore the LPCs which were used in the pointing measurement along with the contribution from the traditional pointing model have to be included. So

$$A_{\text{tel}} = A_{*} - (A_{\text{tm}} + A1_{\text{lpc}} \text{Cos}(E) + A2_{\text{lpc}} + \Delta A) / \text{Cos}(E) \quad (6)$$

and

$$E_{\text{tel}} = E_{*} - (E_{\text{tm}} + E1_{\text{lpc}} + \Delta E) \quad (7)$$

where $(A_{\text{tm}}, E_{\text{tm}})$ are the contributions from the traditional pointing model and $(A1_{\text{lpc}}, A2_{\text{lpc}}, E1_{\text{lpc}})$ are the local pointing corrections.

3 Results

The observations are summarized in Figures 1 and 2. The data are divided into day and night with 153 and 293 observations, respectively. The weather conditions varied throughout the observing period and $\sim 30\%$ of the data were excised because of poor baselines. Also, RFI was detected in about 10% of the data. Nonetheless, the sky coverage is good for both data sets.

The program TPOINT was used to perform a multi-dimensional least-squares fit to the data (Wallace 1998). A traditional pointing model which included 8 physical terms was used. The results for the combined data set are shown in Tables 1 and 2 for the azimuth and elevation series, respectively. The results of this TPOINT analysis are shown as a series of plots (Figures 3–8).

The sky root-mean-square (*rms*) is $7''.4$. This is slightly better than the S-band observations at 2 GHz ($rms = 8''.5$), probably due to the improvements in focus-tracking and refraction. The data were divided into day and night and analyzed separately to probe for any temperature dependent effects. The observations consisted of two days and three nights producing an *rms* of $6''.8$ and $7''.4$, respectively. The pointing coefficients are similar between the two data sets. Although the ambient temperature is warmer during the day than at night it varies significantly between days (see Figure 9). Therefore it would be difficult to detect the focus tracking temperature dependent effects. Figure 9 indicates temperature variations between 10–15 Celsius which, theoretically, should produce pointing errors of $\sim 18''$. The measured *rms* appears lower than would be expected from theory.

Table 1: Azimuth Pointing Terms ($\Delta A \cos E$)

Coeff. (M&C)	Coeff. (TPOINT)	Term	Value (arcsec)	σ (arcsec)	Meaning
$d_{0,0}$	-CA	1	-29.82	6.221	Horizontal Collimation
$b_{0,1}$	-NPAE	Sin E	-3.57	4.451	El Axle Collimation
$d_{0,1}$	-IA	Cos E	-11.71	4.943	Az Zero
$b_{1,1}$	AW	Cos A Sin E	+2.20	0.422	Zenith E-Tilt
$a_{1,1}$	AN	Sin A Sin E	+2.97	0.431	Zenith N-Tilt

Table 2: Elevation Pointing Terms (ΔE)

Coeff. (M&C)	Coeff. (TPOINT)	Term	Value (arcsec)	σ (arcsec)	Meaning
$d_{0,0}$	IE	1	-758.47	6.226	El Zero
$c_{1,0}$	-AW	Sin A	-2.20	0.422	Zenith E-Tilt
$d_{1,0}$	AN	Cos A	+2.97	0.431	Zenith N-Tilt
$b_{0,1}$	ECES	Sin E	+678.13	4.443	Asymmetric Gravity
$d_{0,1}$	ECEC	Cos E	+795.03	4.925	Symmetric Gravity

Figure 8 plots the zenith angle residuals versus zenith angle. Any significant errors in the refraction model should be revealed in this plot. There appear to be no major problems at least to within the accuracy of these measurements. An extra pointing coefficient of the form $\text{Cot}(E)$ was added to the elevation series which would reveal any scaling errors in refraction. This pointing coefficient was determined to be only $1''.23 \pm 0.425$.

It has been suggested that additional pointing coefficients due to irregularities in the azimuth track should be investigated for the GBT (Condon, GBT Memo 75). These have the form of $\text{Sin}(2A)\text{Cos}(E)$ and $\text{Cos}(2A)\text{Cos}(E)$ in the azimuth series. Including these terms slightly reduces the overall *rms* to $7''.3$; the coefficients are $1''.07 \pm 0.728$ and $1''.95 \pm 0.834$, respectively. They are essentially on the same order as the azimuth track tilt terms.

Inspection of Figure 5 ($\Delta A \text{Cos} E$ as a function of azimuth) reveals sinusoidal features in the residuals. Adding pointing terms to the azimuth series of the form $\text{Cos}(A)$ and $\text{Sin}(A)$ produces coefficients with amplitude $3''.17 \pm 0.575$ and $0''.99 \pm 0.558$, respectively. The residuals in Figure 5 appear flatter and the all sky *rms* is reduced to $7''.1$. Similar improvements can be made by adding the azimuth centering error coefficients of the form $\text{Cos}(A)\text{Cos}(E)$ and $\text{Sin}(A)\text{Cos}(E)$ to the azimuth series. However, including any of the additional terms thus far suggested beyond the 8 physical terms listed in Tables 1 and 2 does not significantly improve the solution at the 5% level when applying the F test.

The calculated pointing coefficients given in Tables 1 and 2 are significantly different than those previously determined at S-band (see GBT Com. Memo 6). The horizontal collimation ($d_{0,0}$), the elevation axle collimation ($b_{0,1}$), and the azimuth zero ($d_{0,1}$) in the azimuth series are significantly different. This is because a different focus tracking model was used between the two pointing runs. Notice that for the X-band data the elevation axle appears to be aligned to within a few arcsec although the three coefficients are highly coupled. The track terms are consistently only a few arcsec in both models. The elevation zero ($d_{0,0}$), the asymmetric gravity ($b_{0,1}$), and the symmetric gravity ($d_{0,1}$) in the elevation series are overall the largest terms. They are slightly reduced for the X-band data probably because the refraction model has been improved, although these three terms are highly correlated (see the correlation matrix shown below).

IE	-0.0005						
NPAE	+0.9401	+0.0006					
CA	-0.9878	+0.0002	-0.9781				
AW	+0.0457	-0.0590	+0.0115	-0.0395			
AN	+0.0114	+0.0450	+0.0117	-0.0136	-0.0171		
ECEC	-0.0000	-0.9875	-0.0007	+0.0002	+0.0462	-0.0430	
ECES	+0.0011	-0.9779	-0.0002	-0.0008	+0.0633	-0.0179	+0.9393

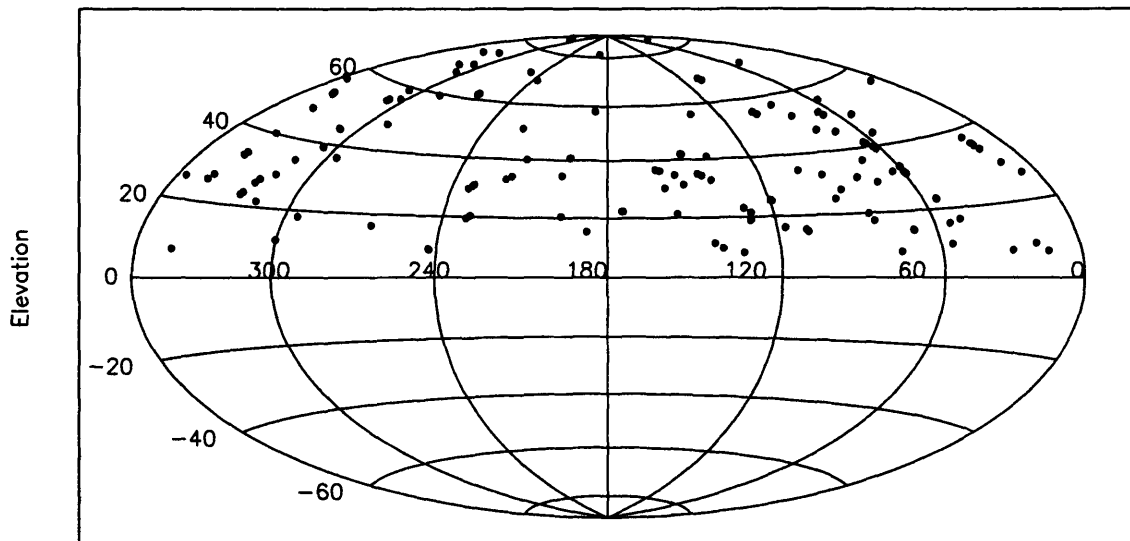
IA	IE	NPAE	CA	AW	AN	ECEC
----	----	------	----	----	----	------

4 Conclusion

An all sky pointing run was performed at X-band (9.6 GHz) which incorporated a refined model for both focus tracking and refraction. A traditional pointing model including 8 physical terms produces an *rms* of $7''.4$. There was no large difference in the pointing model between day and night, although this would have been difficult to detect given the weather data.

Additional pointing terms were also investigated. Irregularities in the azimuth track of the form $\text{Sin}(2A)\text{Cos}(E)$ and $\text{Cos}(2A)\text{Cos}(E)$ were measured to be on the order of $\sim 1-2''$. A $\text{Cot}(E)$ term was used to probe for scaling errors in the refraction model which were determined to be $\lesssim 1''$.

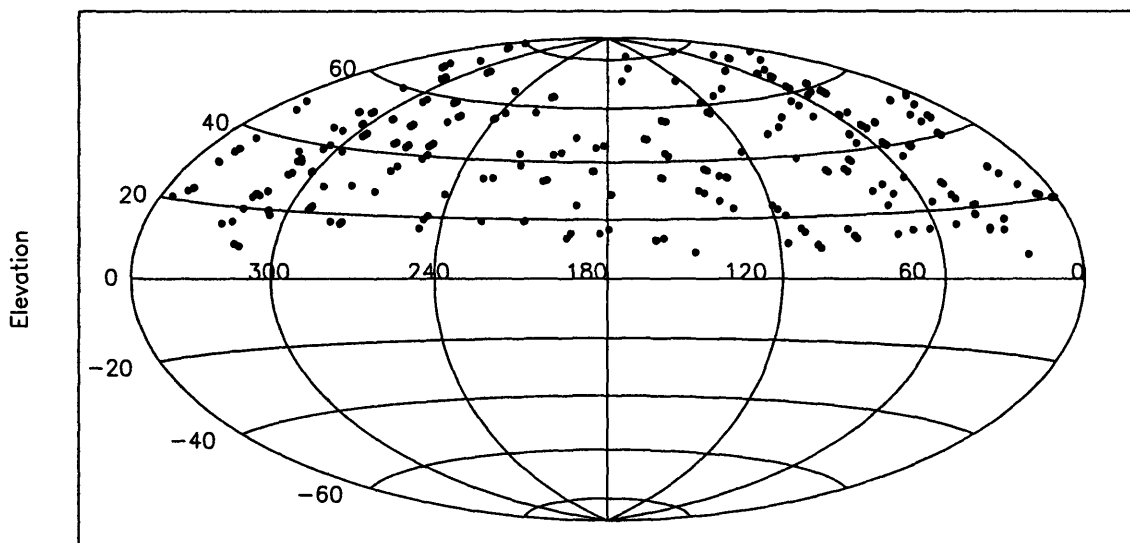
GBT X-band 28–30 December (Daylight) [point_xband_04]



Azimuth centered on 180

Figure 1: Distribution of sources on the sky with an aitoff projection for project point_xband_04 during only daylight.

GBT X-band 28–30 December (Night) [point_xband_04]



Azimuth centered on 180

Figure 2: Distribution of sources on the sky with an aitoff projection for project point_xband_04 during only night.

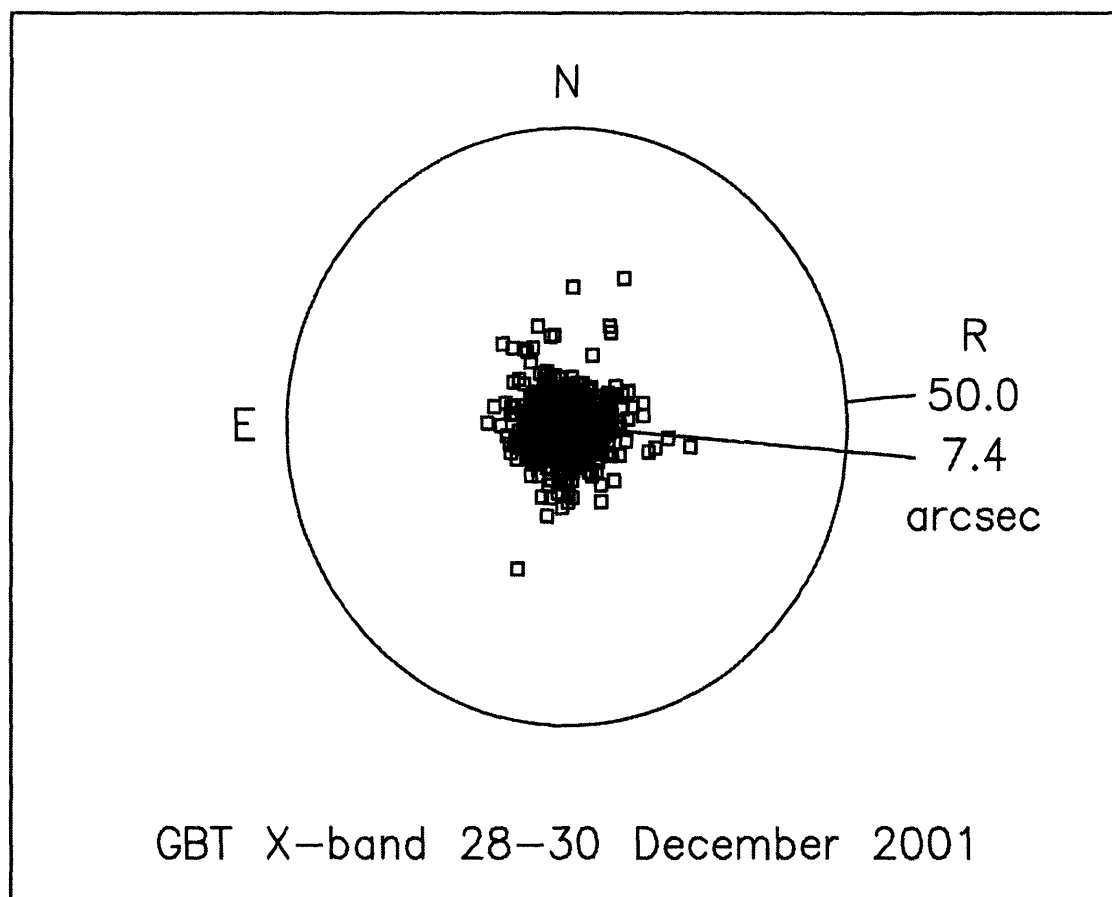


Figure 3: The residuals plotted as a scatter diagram. The inner circle is the sky *rms* of the fit (7".4).

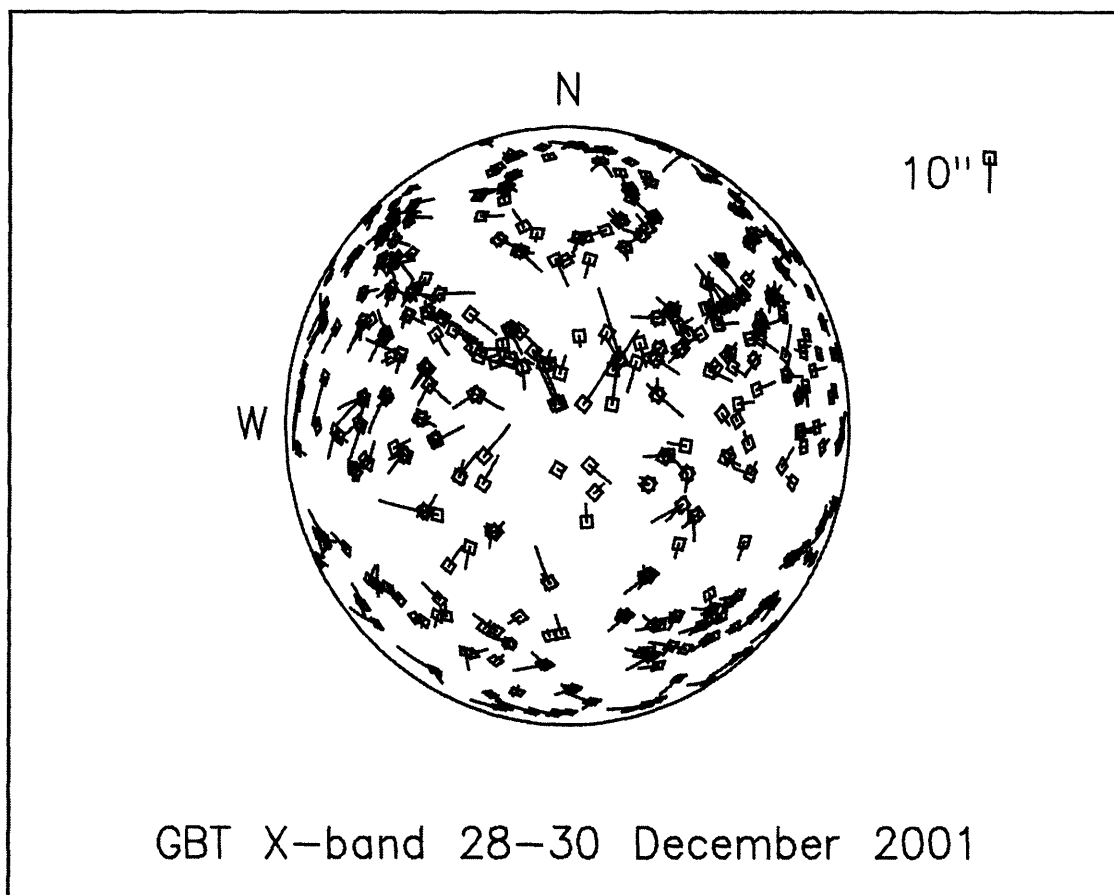


Figure 4: The pointing residuals as error vectors on an azimuthal projection.

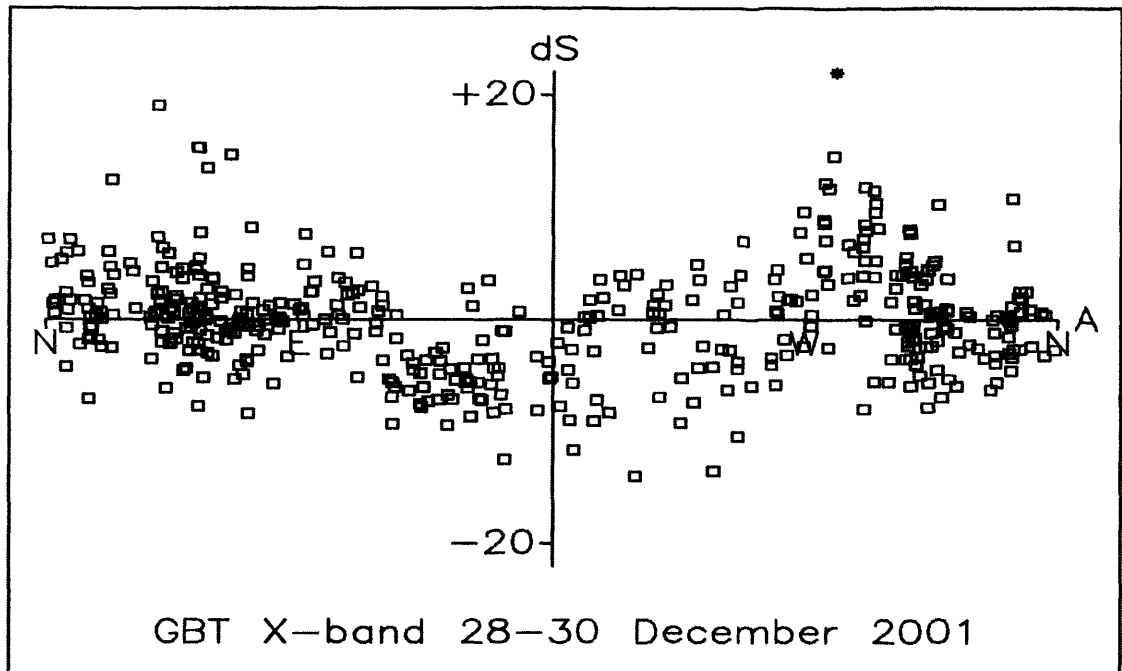


Figure 5: The pointing error horizontally on the sky ($\Delta A \cos E$) as a function of azimuth.

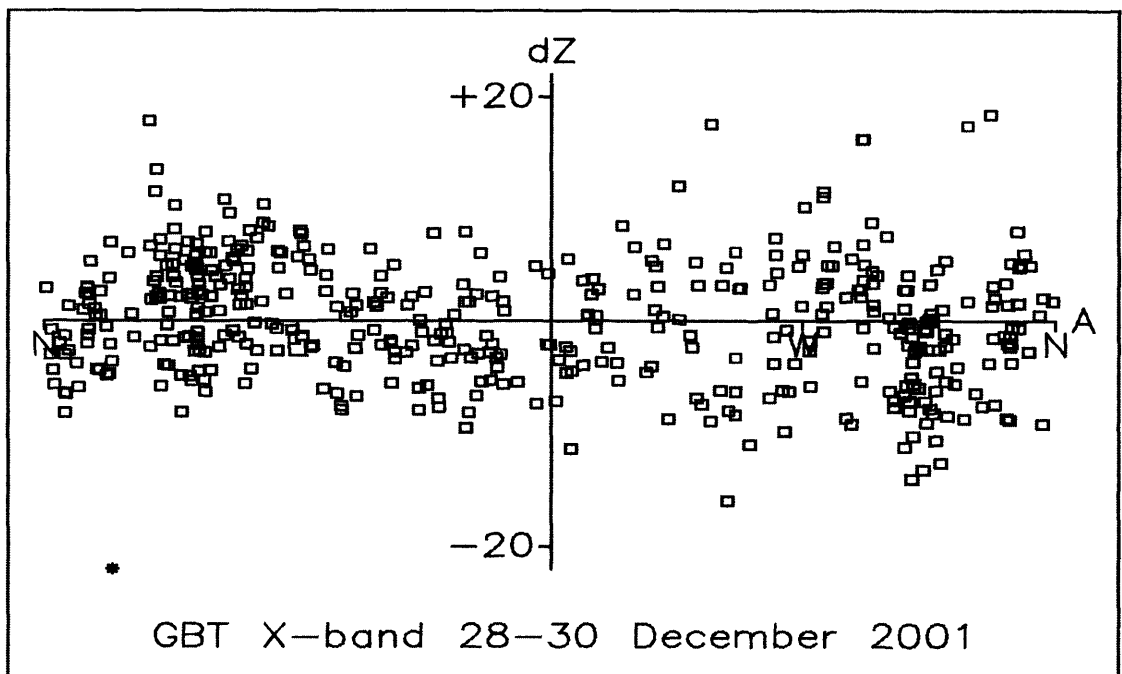


Figure 6: The pointing error in zenith angle as a function of azimuth.

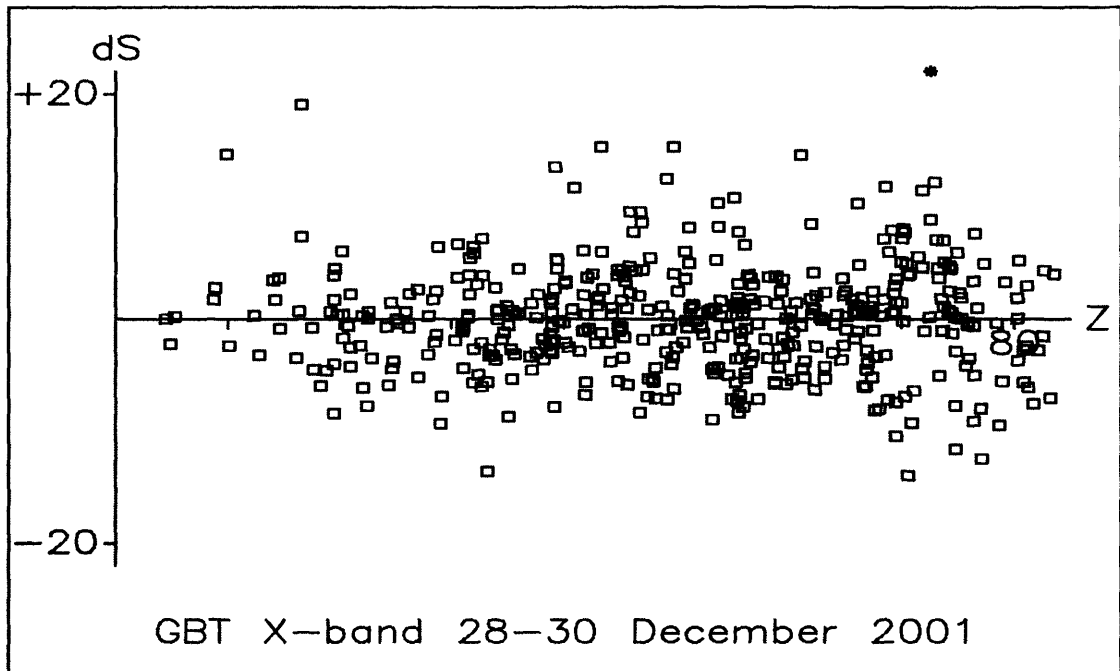


Figure 7: The pointing error horizontally on the sky ($\Delta A \cos E$) as a function of zenith angle.

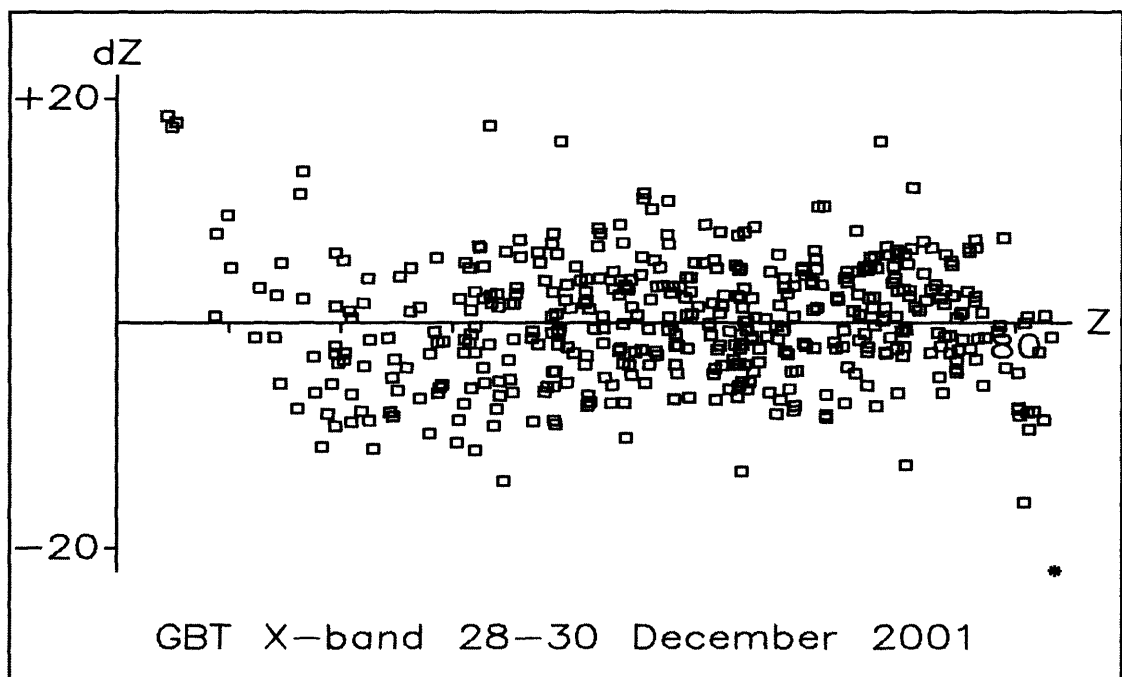


Figure 8: The pointing error in zenith angle as a function of zenith angle.

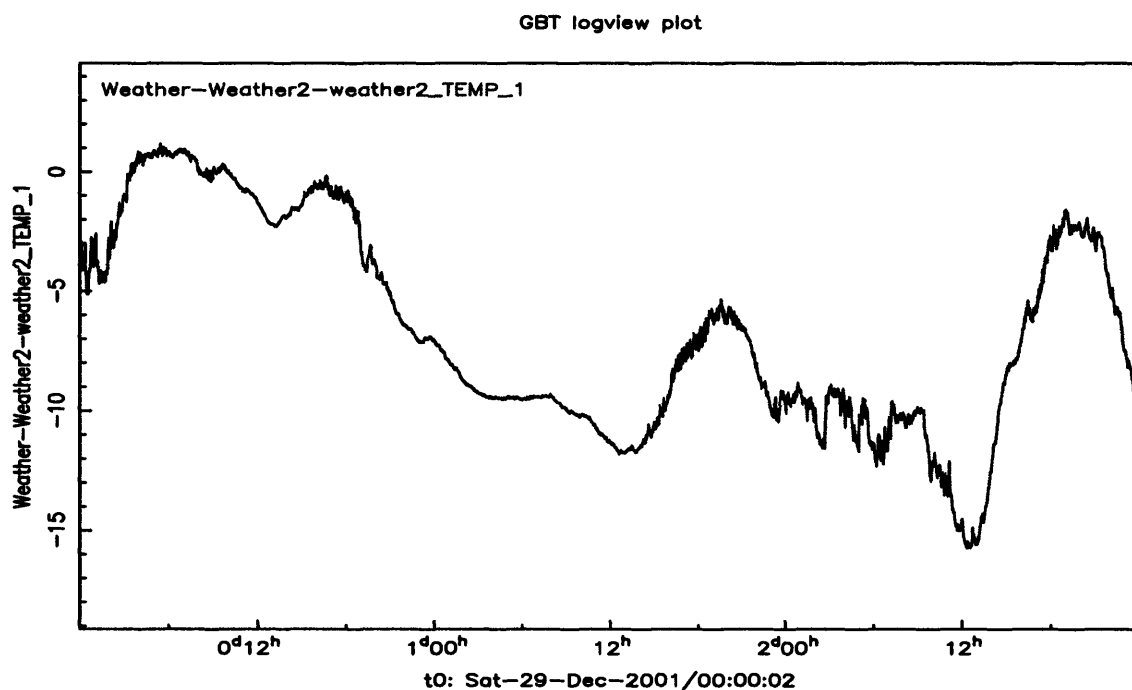


Figure 9: The ambient temperature in Celsius as a function of UT. Note that daylight occurs between 12:40 until 22:15 UT and correlate with an increase in temperature.